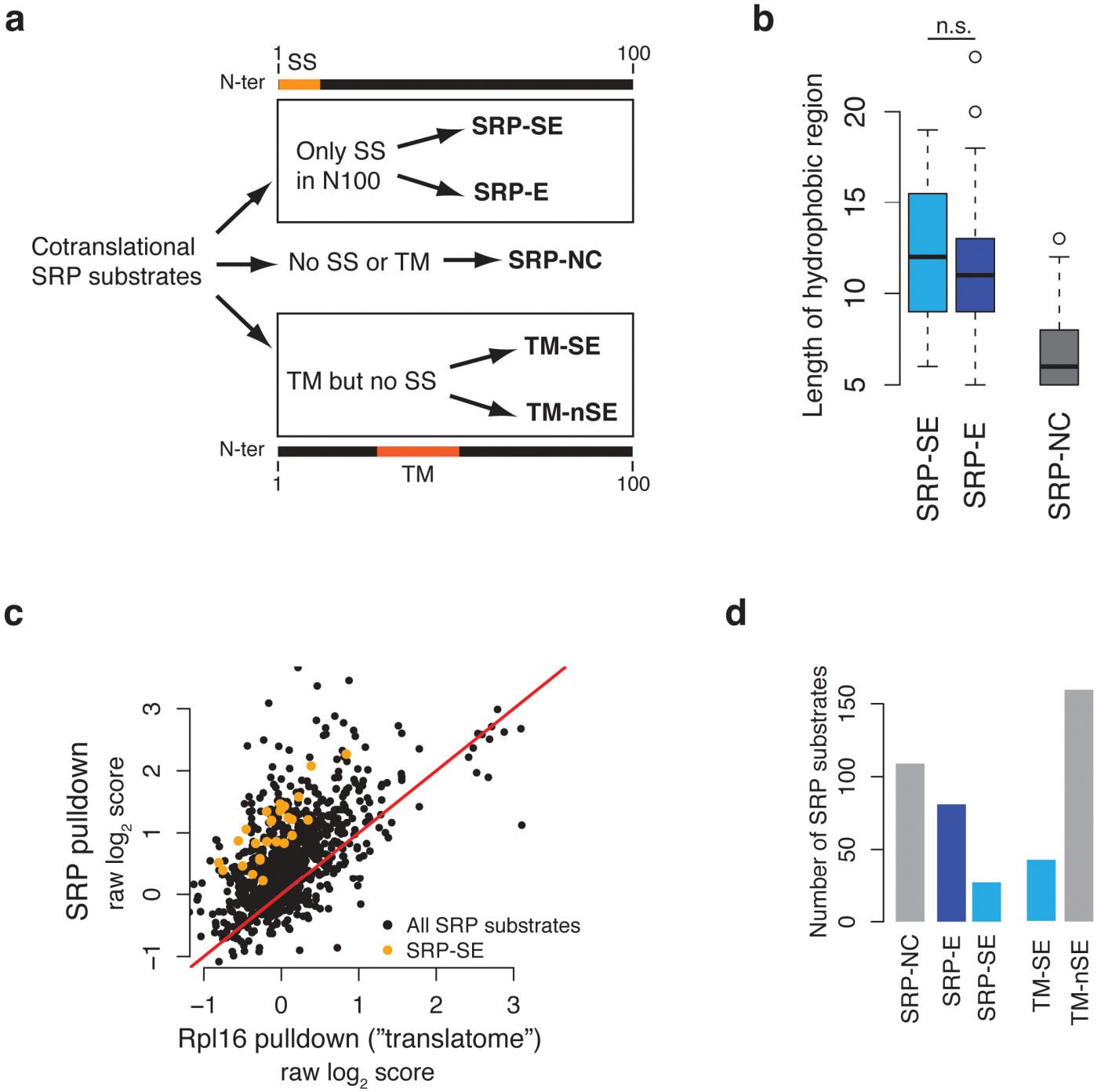

Supplementary Figure 1

Classification of cotranslational SRP substrates.

a, Schematic overview of the classes of cotranslational SRP substrates analyzed in this study. **b**, Distributions of the length of the hydrophobic region in the SS for SRP-SE and SRP-E proteins. For SRP-NC proteins, we show the lengths of the first stretch of at least 5 hydrophobic amino acids. **c**, Comparison of the SRP pull-down to the translatome highlights enrichment in SRP interaction relative to the level of translation. Strongly enriched SS-proteins (SRP-SE) are shown in orange. **d**, Overview of the number of SRP substrates in each class.

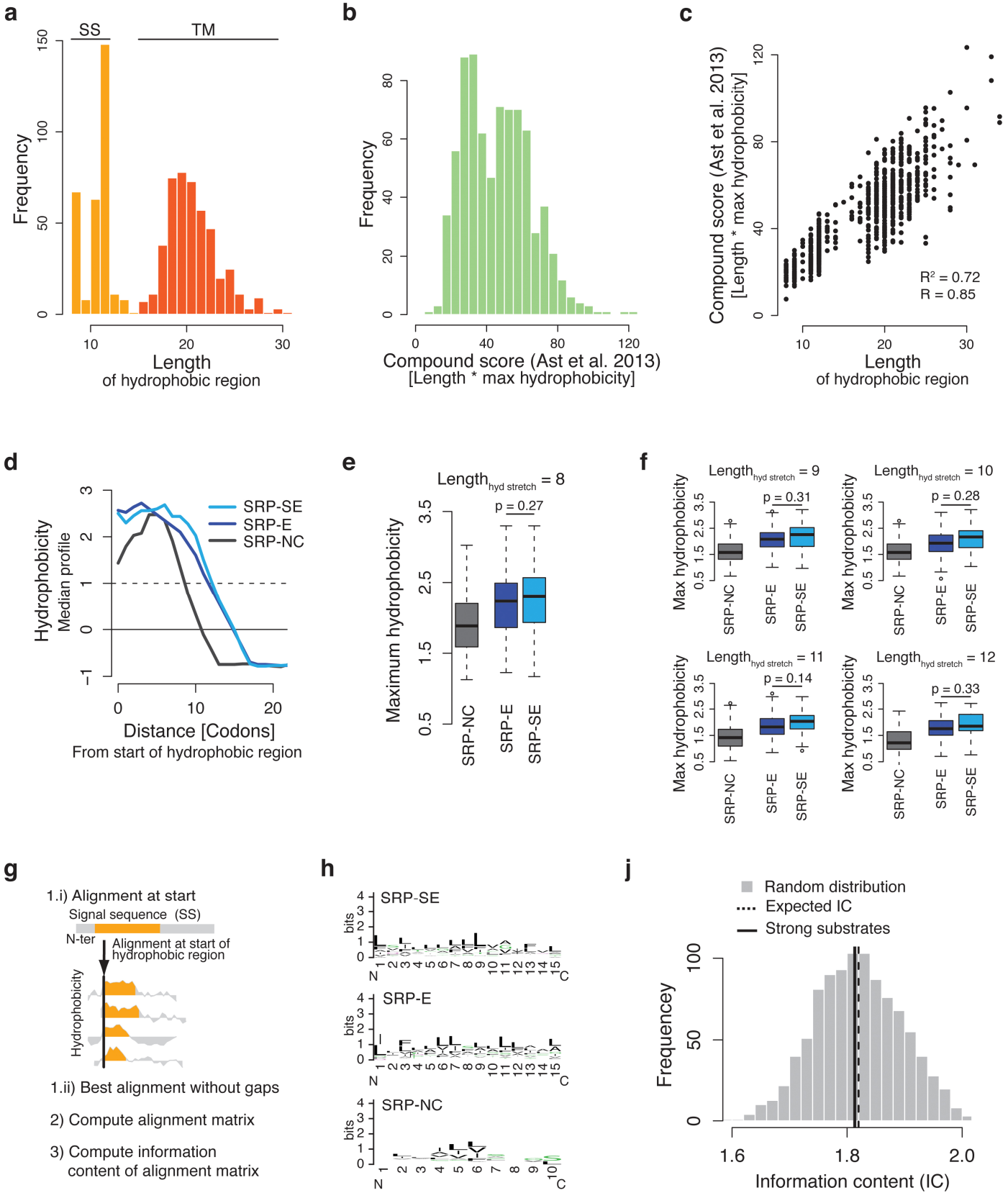

Nature Structural and Molecular Biology: doi:10.1038/nsmb.2919

Supplementary Figure 2

Hydrophobicity or putative sequence motifs alone cannot explain SRP enrichment.

a, Histogram of the length of the hydrophobic region in SS and TM segments. **b**, A compound score is defined as the product of the maximum hydrophobicity and the length of the hydrophobic region in SS or TM segments. Shown is the histogram of the compound score for all cotranslational SRP substrates. **c**, The compound score is highly correlated with the length of the hydrophobic region as its strongest determinant. **d**, Representative median hydrophobicity profiles of the SS of SRP-SE (n=29) and SRP-E (n=78) substrates, and longest N-terminal hydrophobic stretch for SRP-NC (n=109) substrates. **e**, Distributions of the most hydrophobic stretch of length 8, possibly the optimal SRP binding site, within the SS of SRP-E and SRP-SE proteins indicate no significant global differences in hydrophobicity. **f**, The most hydrophobic region of length 9–12 in the SS or N-terminal hydrophobic stretches is identified, and the distributions for SRP-SE, SRP-E and SRP-NC proteins compared. Independent of the length of the region considered, SRP-SE SS are not significantly more hydrophobic than SRP-E SS. **g**, Schematic overview of the quantification of possible sequence motifs in the hydrophobic regions of SS. In separate analyses, the sequences are aligned either at the start of the hydrophobic region, or as the best local alignment without gaps. From the sequence alignments, sequence logos, the alignment matrix and the information content (IC) are computed. **h**, Sequence logos of the hydrophobic binding sites in SRP-NC, SRP-E and SRP-SE substrates show no distinct sequence motifs for SRP-SE proteins that may explain their stronger enrichment. **j**, Distribution of the IC of the hydrophobic region in random subsets of SS-proteins. Because the IC for the SRP-SE proteins (solid line) falls very close to the expected mean of the random distribution (dotted line) instead of being clearly shifted to the right, we conclude that there is no pronounced sequence motif in the hydrophobic regions of SS that sets SRP-SE substrates apart and may explain their higher enrichment scores.

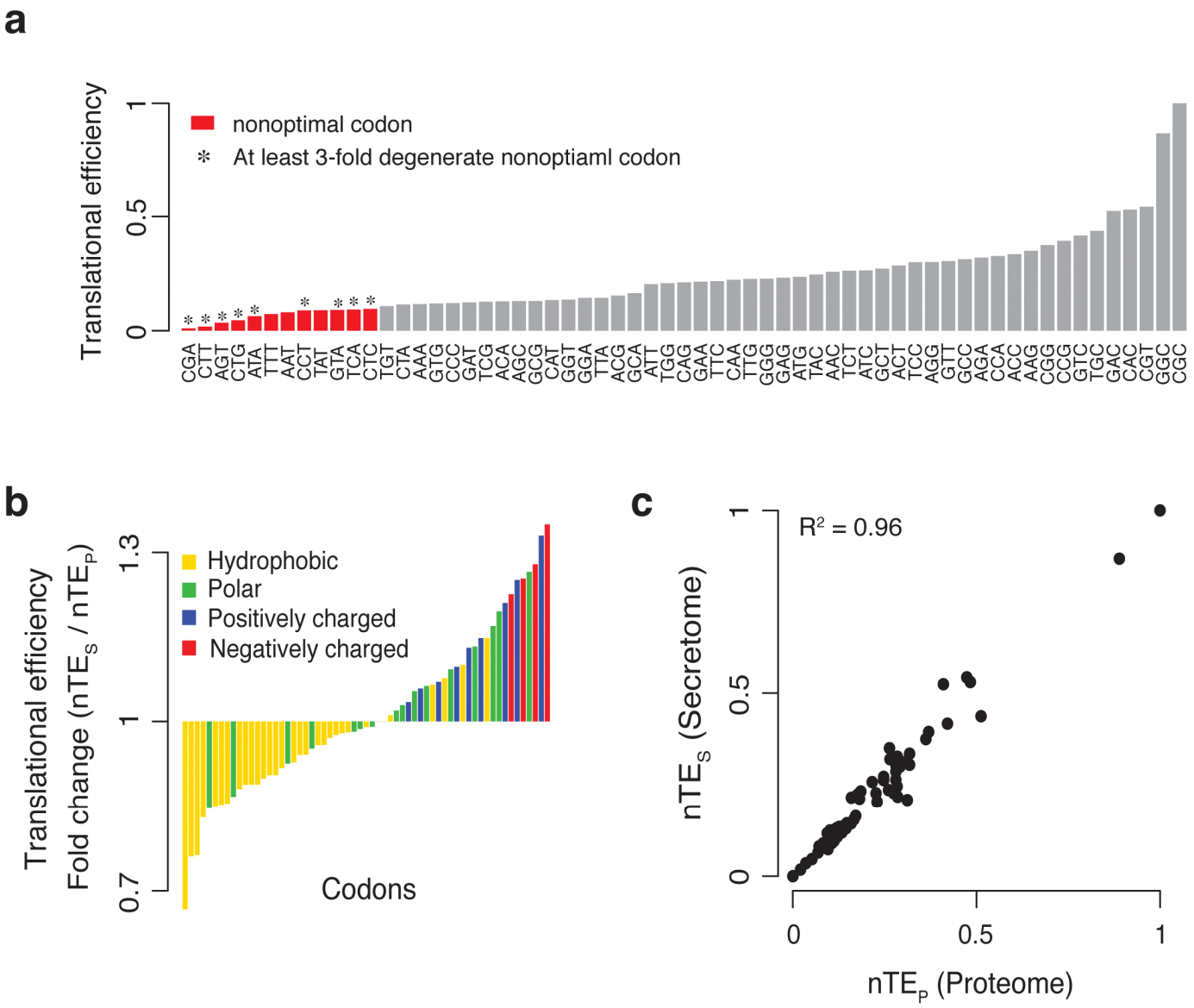

Supplementary Figure 3

Translational efficiency (TE) of translocated proteins.

a, Because secretory and trans-membrane proteins are translated in a spatially-organized manner at or near the ER membrane, we derived a scale of codon-specific TEs based on the availability of the cellular tRNA pool and the codon usage of the secretome. The 20% lowest efficiency codons were defined as “nonoptimal”. Nonoptimal codons that are at least 3-fold degenerate are indicated by “*”. **b**, The normalized TE scales that incorporate the codon usage of the full proteome (nTE_P), and, alternatively only the codon usage of the secretome (nTE_S), differ as predicted: codons encoding hydrophobic amino acids become less efficient, and those encoded charged residues become more efficient. However, the differences, show by per-codon fold changes, are relatively small. **c**, The nTE_P and nTE_S scales are very highly correlated and lead to identical definitions of nonoptimal codons. This analysis served to validate that our results are robust, irrespective of predicting the TE for the full proteome or only secreted and trans-membrane proteins.

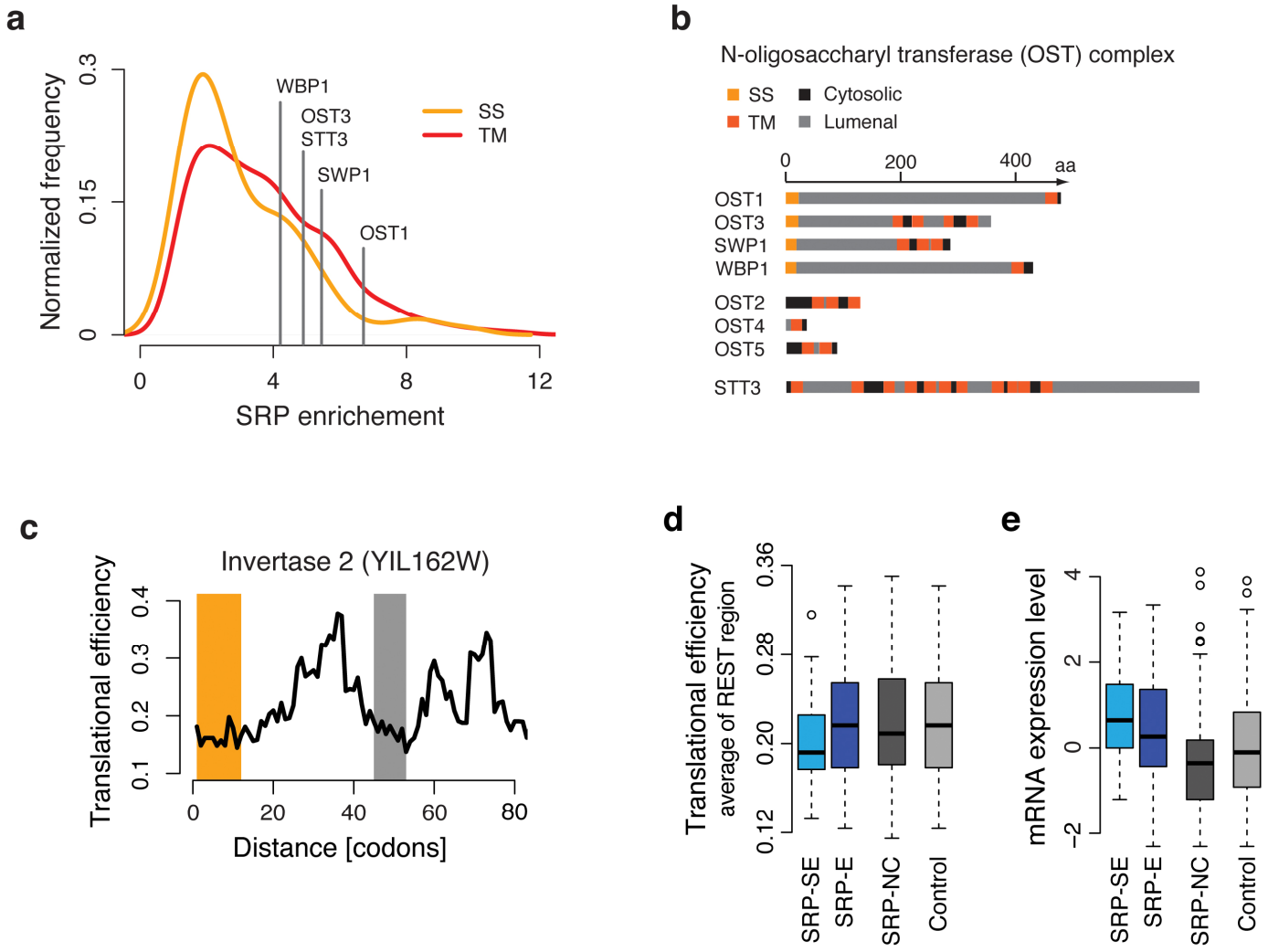

Supplementary Figure 4

SRP recognition of SS proteins.

a, SRP-dependent translocation of the essential N-oligosaccharyl transferase (OST). OST subunits are some of the most enriched SRP substrates. **b**, Four of eight OST subunits, namely Ost1, Ost3, Swp1, and Wbp1 have a distinct structure of a SS followed by a long lumenal domain. The topology of the other four subunits, Ost2, Ost4, Ost5, and Stt3 are shown for comparison. **c**, The coding sequence of Invertase, the model substrate that could accommodate many random sequences as functional SS, is characterized by a very pronounced region of low TE (grey bar) ca. 45 codons downstream of the start of the hydrophobic region of the SS (yellow bar). **d**, Distribution of average predicted translational efficiencies 38-45 codons downstream of the start of the signal sequences for strongly-enriched (SRP-SE) and enriched (SRP-E) cotranslational SRP substrates compared to the average predicted translational efficiencies 38-45 codons downstream of N-terminal hydrophobic stretches in non-cognate SRP substrates (SRP-NC) and cytosolic proteins that do not bind to SRP (Control). **e**, mRNA expression levels (log scale) of SRP-SE, SRP-E, SRP-NC and Control genes. While TE generally correlates with expression, the strong dip in TE in SRP-SE substrates is not confounded by expression. SRP-NC substrates may interact non-canonically because they are translated generally more slowly linked to their lower levels of expression.

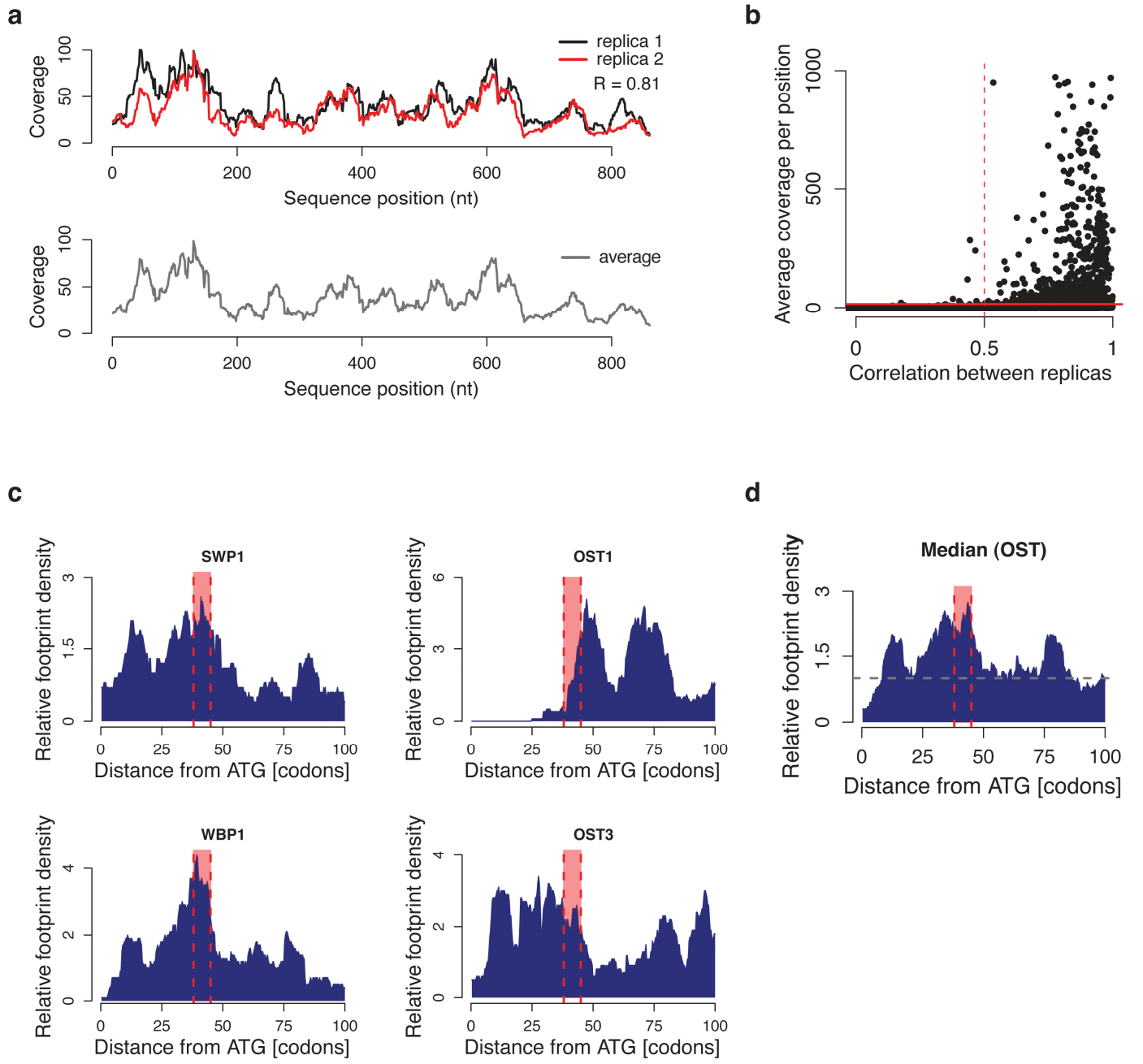

Supplementary Figure 5

Ribosome profiling analyses of SRP substrates.

a, Exemplary ribosome footprint density profiles for two replicas (top), and the resulting average profile (bottom). Plotted are the sequenced footprints per position. **b**, Relationship between average coverage and correlation between replicas in the analyzed ribosome profiling dataset. A minimum average coverage of ten sequencing reads per position eliminates many cases of very low reproducibility. **c**, Relative footprint density profiles for the OST subunits with SS. **d**, The median relative footprint density profile for the OST subunits reflects the consistent characteristics of the individual profiles.

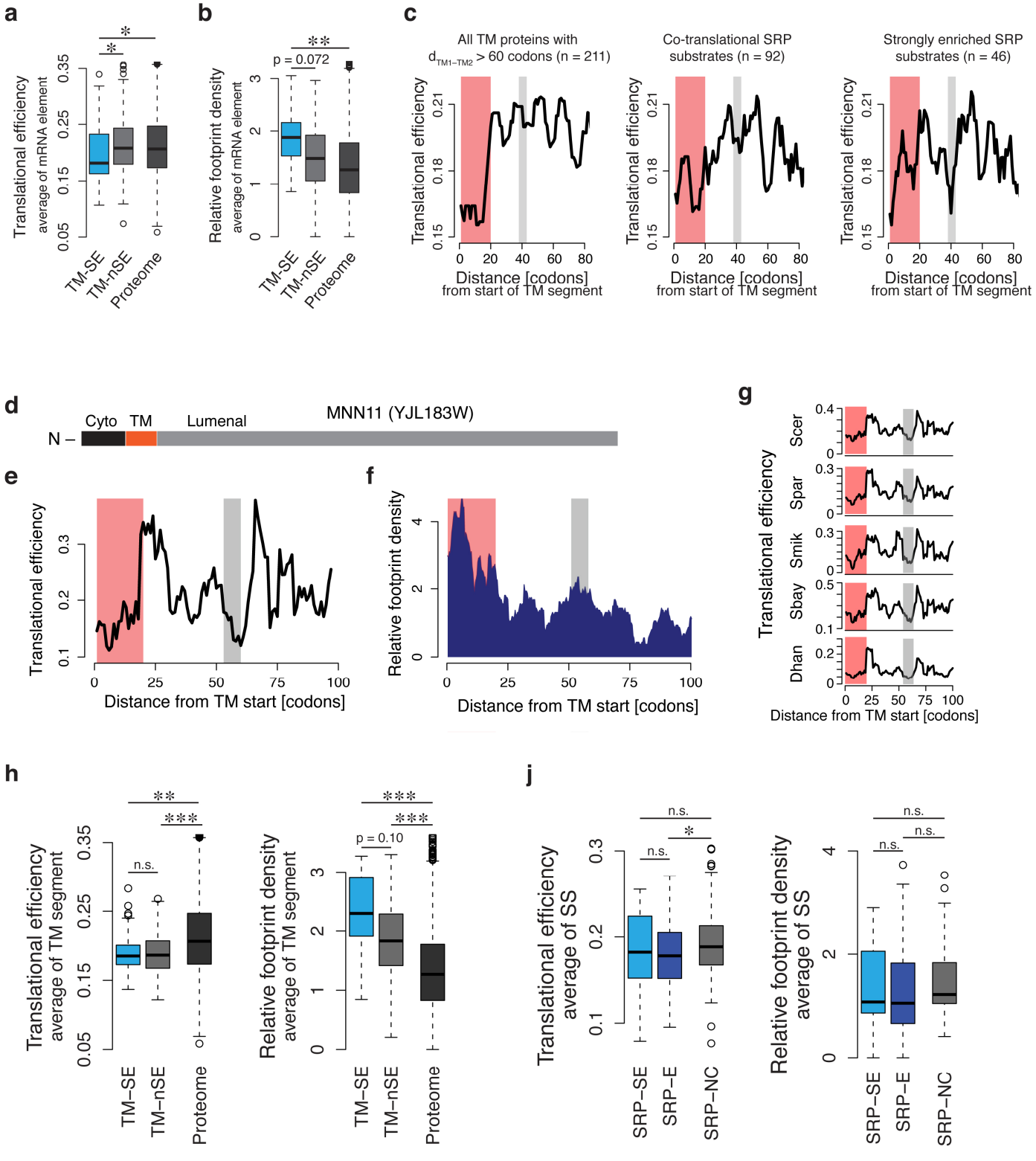

Supplementary Figure 6

Analysis of REST sequences in TM proteins.

a, The average TE of individual TM-SE profiles (n=46) in the translational slowdown element downstream of the TM segments is significantly lower than in TM-nSE (n=165) substrates (Wilcoxon rank-sum test: p = 0.045). **b**, Distributions of the average footprint densities in the translational slowdown element is higher in TM-SE proteins (n=14) than in TM-nSE proteins (n=27), but the difference is not significant (Wilcoxon rank-sum test: p = 0.072). **c**, The translational slowdown element downstream of TM helices is more pronounced for more strongly enriched SRP substrates. Shown are medium TE profiles for all TM-proteins with $d_{TM1-TM2} > 60$ codons including those that do not significantly interact with SRP cotranslationally, only those that significantly interact with SRP cotranslationally, and those that are strongly enriched in SRP binding. **d**, The alpha-1,6-mannosyltransferase MNN11 has a single signal-anchor TM domain near the N-terminus that acts as SRP binding site. The region downstream of the TM, which is translated when the TM domain has emerged from the ribosome exit tunnel, is characterized by: **e**, locally low predicted translational efficiency, and **f**, high ribosome footprint density. Both the lower translational efficiency and the higher footprint density are observed ca. 55-60 codons downstream of the start of the TM, allowing the full TM domain to emerge from the ribosome exit tunnel. **g**, The distinct translational efficiency profile of MNN11 is evolutionarily conserved across yeasts, here shown for the closely related *S. paradoxus*, *S. mikatae*, *S. bayanus*, and *D. hansenii*. **h**, The average TE of TM segments themselves is comparable between TE-SE and TE-nSE proteins, but significantly lower than the average across the proteome. In agreement, the average footprint densities of the TM segments in TM-SE and TM-nSE substrates are significantly higher than for random regions of the same length across the proteome. Of note, the first TM segments of the TM-SE proteins are also on average characterized by higher footprint densities than the first TM segments in the TM-nSE proteins. **j**, Both predicted TE and experimental footprint densities of the SS themselves do not differ between SRP-SE and SRP-E proteins. Differences between distributions are tested by the Wilcoxon rank-sum test, and significance levels are indicated as *: $p < 0.05$; **: $p < 0.01$; ***: $p < 0.001$.

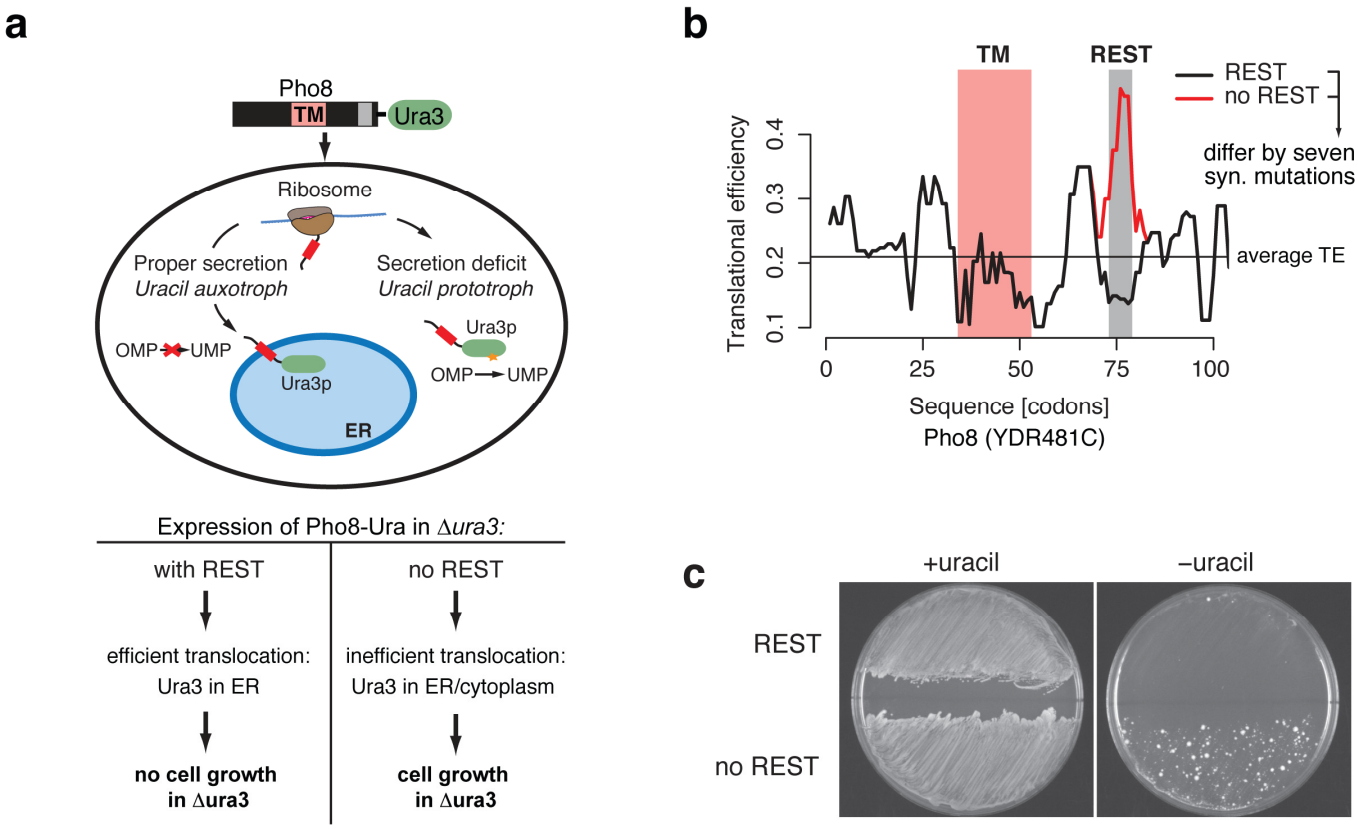

Supplementary Figure 7

Loss of REST element causes translocation defect.

a, Translocation assays were performed as described in Dalley *et al*. (*Mol Biol Cell*, 2008). The plasmid pMP211 was kindly provided by Martin Pool (University of Manchester, UK). This pRS314-derived vector encodes an open reading frame, under control of the PHO5 promoter, comprising the first 82 residues of *S. cerevisiae* Pho8p fused to the amino terminus of the complete *S. cerevisiae* Ura3p. Proper secretion localizes Ura3p to the ER lumen where it cannot access its substrate orotidine-5′-phosphate (OMP) to produce uridine monosphosphate (UMP). Secretion deficiencies accumulate functional Ura3p in the cytosol conferring uracil prototrophy. **b**, Synonymous mutations improving translational efficiency within the REST region of Pho8p were introduced, converting the sequence 5′-ATATTCTTCGTGACGGATGGAATGGGACCT-3′ to 5′-AT**C**TTCTTCGT**C**AC**C**GA**C**GGCATGGG**C**CC**G**-3′. **c**, Plasmids were transformed into BY4741 and grown on synthetic defined agar with or without uracil. Colonies began to appear with the no-REST plasmid after two days and continued to accumulate over a week (shown at day 6), indicating Ura3 accumulation is stochastic. After 7 days, colonies began to appear with the REST plasmid. Plasmids were recovered from five colonies of varying size from each strain and sequenced. No mutations occurred within the open reading frames, promoter, or untranslated regions.